IEEE Access
Multidisciplinary | Rapid Review | Open Access Journal

Received January 16, 2019, accepted January 30, 2019, date of publication March 14, 2019, date of current version March 26, 2019.

Digital Object Identifier 10.1109/ACCESS.2019.2899456

Control of Powers for Wind Power Generation and Grid Current Harmonics Filtering From Doubly Fed Induction Generator: Comparison of Two Strategies

ADSON BEZERRA MOREIRA[1], TÁRCIO ANDRÉ DOS SANTOS BARROS[2], (Member, IEEE), VANESSA SIQUEIRA DE CASTRO TEIXEIRA[1], RAMON RODRIGUES DE SOUZA[2], MARCELO VINICIUS DE PAULA[2], (Student Member, IEEE), AND ERNESTO RUPPERT FILHO[2]

[1]Department of Electrical Engineering, Federal University of Ceará, Sobral 62010-560, Brazil
[2]Faculty of Mechanical Engineering, University of Campinas, Campinas 13083-740, Brazil

Corresponding author: Tárcio André Dos Santos Barros (tarcioandre@hotmail.com)

This work was supported by the São Paulo Research Foundation, FAPESP under Grant 2017/21640-9, Grant 15/03248-9, and Grant 16/08645-9.

ABSTRACT Two strategies for wind power systems that simultaneously adjust the powers generation from doubly fed induction generator and achieves grid currents harmonic filtering are presented in this paper. The harmonic mitigation function is developed by algorithms proposed for compensating harmonics from the grid side converter. The quality of power is substantially enhanced. The generator side converter regulates the active and reactive powers that are supplied to the electric grid by the stator flux oriented control. This paper presents a novel control system for power generation and electric grid harmonic compensation, which is described and validated through comparison with other strategies. A harmonic filtering behavior analysis for some operation points using the novel strategy is presented. The proposed system efficiency is verified through simulation and experimental results. The grid current THD when none of the proposed strategies are applied is 17.21%. The THD is reduced to 5.68% when strategy 1 is applied. When strategy 2 is used the THD is decreased to 3.18%.

INDEX TERMS Controllers design, doubly fed induction generator, integrated active filter, harmonic filtering, power quality, wind power generation.

I. INTRODUCTION

Modern wind power plants actively participate on the energy quality enhancement. In addition to generating electricity, the wind power plants can mitigate the electrical current harmonics coming from existent nonlinear loads in the same electric grid [1]. Active power filter (APF) is extensively used for mitigating harmonics currents in the electric grid because it detects the harmonic currents caused by nonlinear loads and compensates it by injecting a certain current.

APF based applications have been developed through modifications in DFIG (Doubly Fed Induction Generator) converters control that mitigate most harmonic currents [1]–[7], improving the power quality supplied. References [2] and [3] propose a rotor side converter (RSC) control strategy that realizes reactive power compensation and grid current harmonics filtering of 5th and 7th orders. Although [2] and [3] have similar drive systems, reference [3] employs a priority management among the harmonic filtering function and the maximum power point tracking (MPPT).

The researches [1], [4]–[6] suggest a DFIG/APF system capable of controlling active and reactive power and achieves harmonic current filtering, by using a sliding mode control strategy in the RSC. In [1]–[6], the reference currents required for harmonic filtering were produced using the PQ theory for instantaneous power [8]. In [4], a wind power system that mitigates grid current harmonics and controls the active and reactive power is proposed. The strategy uses constant

The associate editor coordinating the review of this manuscript and approving it for publication was Huiqing Wen.

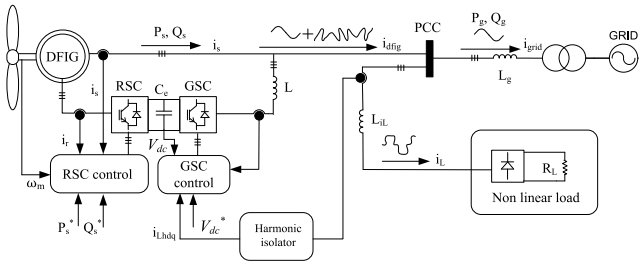

FIGURE 1. Operation design for the proposed DFIG/APF.

switching frequency hysteresis current controllers. The wind power system in [4] and [5] is similar, but it employed a variable switching frequency hysteresis current controller and obtained total harmonic distortion (THD) smaller than in [4].

The grid current harmonics mitigation from RSC control applied in [1]–[7] uses the harmonic currents injection in DFIG. However, this application is not adequate for the machine design leading to an increase in losses, which decrease the machine lifespan. Authors from [7], applied the DFIG with a sensorless vector control, MPPT and grid harmonic current compensation to regulate the generated powers. Other studies developed employed the grid side converter (GSC) with harmonic filter function [9]–[12]. Reference [10] also uses the PQ theory [8] to calculate the reference current for harmonic mitigation while considering the current required by the load. The synchronous reference frame (SRF) theory is widely applied to calculate the reference current [10]–[12]. The SRF theory uses current transformations in the synchronous rotating dq frame [13]. Todeschini and Emanuel [14] compared three different control algorithms by simulation and concluded that it is necessary to combine both RSC and GSC control modulations for filtering and controlling the reactive power.

Swami Naidu and Singh [11], Moreira *et al.* [12] present simulation and experimental results of grid current THD before and after filtering through GSC control. Comparing the results presented in this paper to the results in [11] and [12], we verified that filtering with the strategies proposed in this paper returns lower THD than the results in [12], showing THD lower than 5% as well in [11] according to standard IEEE in [24].

This paper presents a comparative study between two control strategies for a DFIG in a wind-power system. The system topology is depicted in Fig. 1. The presence of a nonlinear load in the point of common coupling (PCC) induces the presence of harmonic currents. The proposed system performs the power control and also filters the current harmonic components of the electric grid current with the GSC. The control of active and reactive generated powers is accomplished by employing the field vector control for the stator.

Two strategies are tested. In strategy 1, the GSC current control uses proportional integral (PI) controllers in the dq frame reference, while in strategy 2, the GSC current control employs proportional multi-resonant current controllers in the $\alpha\beta$ frame reference. In the two strategies, the RSC current control uses PI controllers by rotor current in the dq reference frame. Harmonic current filtering and powers control are performed simultaneously. The SRF theory is applied as harmonic identification method, thus fundamental components extraction is accomplished.

II. POWER CONTROL OF THE DOUBLY FED INDUCTION GENERATOR – DFIG

The dq reference frame is used to control the DFIG in order to decouple the active power from the reactive power of the stator. The stator flux is positioned in the d axis of the reference frame. Equations (1) to (10) express the DFIG mathematical model [15],

$$v_{sd} = r_s i_{sd} + (d\psi_{sd}/dt) - \omega_e \psi_{sq} \quad (1)$$
$$v_{sq} = r_s i_{sq} + (d\psi_{sq}/dt) + \omega_e \psi_{sd} \quad (2)$$
$$v_{rd} = r_r i_{rd} + (d\psi_{rd}/dt) - \omega_{sl} \psi_{rq} \quad (3)$$
$$v_{rq} = r_r i_{rq} + (d\psi_{rq}/dt) + \omega_{sl} \psi_{rd} \quad (4)$$
$$\omega_{sl} = \omega_e - \omega_r \quad (5)$$
$$\psi_{sd} = L_s i_{sd} + L_m i_{rd} \quad (6)$$
$$\psi_{sq} = L_s i_{sq} + L_m i_{rq} \quad (7)$$
$$\psi_{rd} = L_r i_{rd} + L_m i_{sd} \quad (8)$$
$$\psi_{rq} = L_r i_{rq} + L_m i_{sq} \quad (9)$$
$$T_e = 1.5 p L_m \left(i_{sq} i_{rd} - i_{sd} i_{rq}\right) \quad (10)$$

where the d and q indexes refer to the d and q axis of the dq reference frame respectively. The indexes s and r refer to the stator and rotor variables respectively. The variables v, i, r and L are the electric voltage, current, resistance and inductance, ψ is the magnetic flux, ωsl is the slip speed, ωe is the synchronous angular speed while ωr is the synchronous rotational speed. Te is the electromagnetic torque that depends on the number of poles (p).

The mechanical speed of the generator is expressed by (11):

$$\omega_m = 2\omega_r / p \quad (11)$$

The dynamic behavior of the mechanical system depends on the moment of inertia (J), the coefficient of viscous friction (B) and the load torque (T_m). Equation (12) describes the mechanical dynamics of the system.

$$J d\omega_m/dt = T_m - T_e - B\omega_m \quad (12)$$

Assuming that the stator magnetic flux in d and q axis are constant, these values may be expressed as (13) and (14):

$$\psi_{sd} = \psi_s = L_m i_{ms} \quad (13)$$
$$\psi_{sq} = 0 \quad (14)$$

From the flux equations (6) to (9), (13) and (14), one can observe that the stator current components in the dq reference frame can be determined by (15) and (16):

$$i_{sq} = -i_{rq} L_m / L_s \quad (15)$$
$$i_{sd} = (\psi_{sd}/L_s) - i_{rd} L_m / L_s \quad (16)$$

The stator active and reactive powers are defined by (17) and (18) respectively:

$$P_s = 1.5\left(v_{sd}i_{sd} + v_{sq}i_{sq}\right) \tag{17}$$

$$Q_s = 1.5\left(v_{sq}i_{sd} - v_{sd}i_{sq}\right) \tag{18}$$

Replacing (15) into (17), (16) into (18) and considering v_{sd} to be null, the active and reactive power are given by (19) and (20):

$$P_s = -1.5v_s i_{rq} L_m/L_s \tag{19}$$

$$Q_s = 1.5v_s\left(\left(v_s/\omega_e L_m\right) - i_{rd}\right) L_m/L_s \tag{20}$$

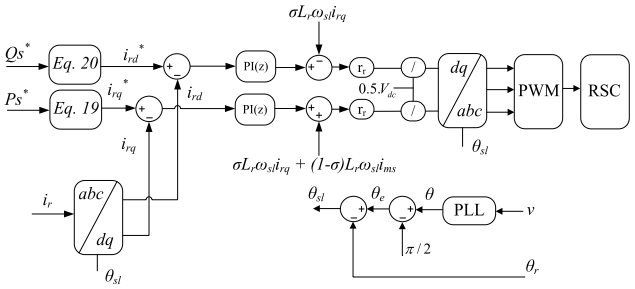

FIGURE 2. Control scheme of RSC.

Equations (19) and (20) imply that the direct and quadrature parcels of the rotor current can be used to control the active and reactive power and to maintain constant voltage at the same time. In Fig. 2, the control scheme for the rotor side converter (RSC) control [15] that regulates the active and reactive powers of the DFIG, where $\sigma = 1 - L_m^2/L_s L_r$ and i_{ms} is the magnetizing current. The PLL (Phase Locked Loop) block generates a θ angle in phase with grid voltage that is handled to synchronize the grid and the converter output voltages. In Fig. 2, the output value, θ_{sl} is the slip angle and is given by (21).

$$\theta_{sl} = \theta - \left(\pi/2\right) - \theta_r, \tag{21}$$

where θ_r is the rotor angle in electrical degrees.

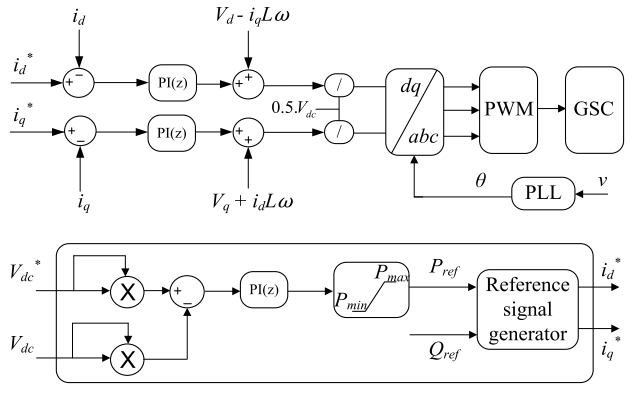

FIGURE 3. Control scheme of GSC.

The GSC control scheme uses current loops for i_d and i_q, taking i_d^* as reference from the DC link voltage control, Fig. 3. Since $i_q^* = 0$, the converter works at a unity power factor. The current references (i_d^*, i_q^*) are generated by the reference signal generator (Fig. 3), from (22) and (23):

$$P_{ref} = 1.5\left[v_d i_d^* + v_q i_q^*\right] \tag{22}$$

$$Q_{ref} = 1.5\left[-v_d i_q^* + v_q i_d^*\right] \tag{23}$$

The reference signal generator block sends i_d^* and i_q^* currents calculated from the desired active and reactive powers, which are, P_{ref} and Q_{ref}, as presented in Fig. 3. Since $v_q = 0$, (22) and (23) can be reduced to (24) and (25):

$$i_d^* = 2P_{ref}/3v_d \tag{24}$$

$$i_q^* = -2Q_{ref}/3v_d \tag{25}$$

III. GSC ACTIVE POWER FILTER – STRATEGY 1

The presence of a nonlinear load in the PCC distorts the grid current. To mitigate this problem, an active filter can be employed to minimize the distortion of the current flowing through the electric grid. In Fig. 5 the control algorithm of the GSC is changed with the addition of i_{Lhd} in the loop i_d and i_{Lhq} in the loop i_q, these changes keep the DC link voltage and allow to compensate the harmonic currents of the grid [12]. The direct (i_d^r) and quadrature (i_q^r) modified reference currents for harmonic compensation are given by (26) and (27):

$$i_d^r = i_d^* + i_{Lhd} \tag{26}$$

$$i_q^r = i_q^* + i_{Lhq}, \tag{27}$$

where the h index indicates the harmonic component of the signal. Thus, i_{Lhd} and i_{Lhq} are the nonlinear load harmonic current components in the dq reference frame, i_d^* and i_q^* are the direct and quadrature grid side converter currents.

Electric grid current filtering is initiated from nonlinear load current measurement and derivation of the desired components that are converted to the dq reference frame (i_{Ld}, i_{Lq}) using equation (28).

$$\begin{bmatrix} i_{Ld} \\ i_{Lq} \end{bmatrix} = 2/3 \begin{bmatrix} \cos\theta & \cos\left(\theta - 2\pi/3\right) & \cos\left(\theta - 2\pi/3\right) \\ -sin\theta & -\sin\left(\theta - 2\pi/3\right) & -sin\left(\theta - 2\pi/3\right) \end{bmatrix} \times \begin{bmatrix} i_{La} \\ i_{Lb} \\ i_{Lc} \end{bmatrix}, \tag{28}$$

where iLd and iLq are direct and quadrature nonlinear load currents.

The nonlinear load currents (iLd, iLq) are treated by a low-pass filter aiming to isolate the fundamental component. The fundamental component of the current is derived from the load current according to equations (29) and (30). The filter cutoff frequency is 12 Hz.

Harmonic components are identified as shown in Fig. 5, then (29) and (30) are summed to the dq reference currents as depicted in Fig. 4.

$$i_{Lhd} = i_{Ld} - i_{Lfd} \tag{29}$$

$$i_{Lhq} = i_{Lq} - i_{Lfq} \tag{30}$$

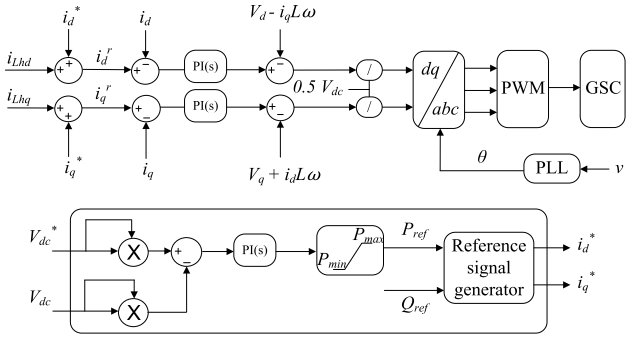

FIGURE 4. GSC active power filter (APF) block diagram – Strategy 1.

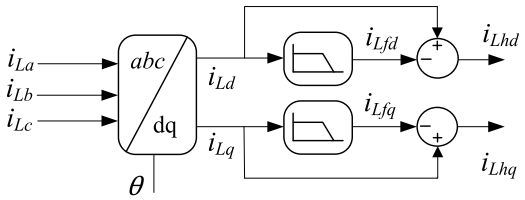

FIGURE 5. Harmonic identifier – Strategy 1.

where iL is the nonlinear load current and the indexes h and f indicate the harmonic and fundamental components of the current, while d and q are the direct and quadrature components of the current in the dq reference frame.

IV. GSC ACTIVE POWER FILTER – STRATEGY 2

This section presents a new proposal. As depicted in Fig. 6, the control structure of the GSC is in the $\alpha\beta$ reference frame, $i_{Lh\alpha}$ and $i_{Lh\beta}$ are added to i_α and i_β in the loop. Also, the DC link voltage is maintained constant and the grid harmonic currents are compensated.

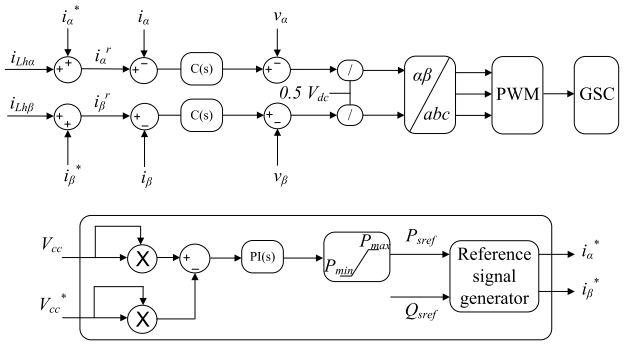

FIGURE 6. Proposed APF scheme in the GSC – Strategy 2.

The harmonic identifier for Strategy 2 is presented in Fig. 7, the reference currents i_α^r and i_β^r, are given by (31) and (32):

$$i_\alpha^r = i_\alpha^* + i_{Lh\alpha} \tag{31}$$

$$i_\beta^r = i_\beta^* + i_{Lh\beta}, \tag{32}$$

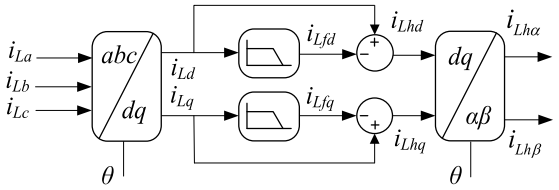

FIGURE 7. Harmonic identifier – Strategy 2.

where $i_{Lh\alpha}$ and $i_{Lh\beta}$ are the nonlinear load harmonic current components in the $\alpha\beta$ reference frame, i_α and i_β are currents of the grid side converter in the $\alpha\beta$ reference frame.

In a similar way to strategy 1, the nonlinear load current measured converted in the dq reference frame (i_{Ld}, i_{Lq}) using equation (28). The fundamental component must be deduced from the load current, and then the harmonic current components are separated from (29) and (30). The harmonic components identified i_{Lhd} and i_{Lhd}, in Fig. 7, are converted to the $\alpha\beta$ reference frame by (33) and combined to the reference currents generated by the reference signal generator in Fig.6.

$$\begin{bmatrix} i_{Lh\alpha} \\ i_{Lh\beta} \end{bmatrix} = \begin{bmatrix} \cos\theta & -sin\theta \\ sin\theta & \cos\theta \end{bmatrix} \begin{bmatrix} i_{Lhd} \\ i_{Lhq} \end{bmatrix} \tag{33}$$

The GSC block diagram uses currents loops to i_α and i_β, having i_α^* and i_β^* as references current from the DC link voltage control, Fig. 6. The reference signal generator produces the current references from (34) and (35):

$$P_{ref} = 1.5\left[v_\alpha i_\alpha^* + v_\beta i_\beta^*\right] \tag{34}$$

$$Q_{ref} = 1.5\left[-v_\alpha i_\beta^* + v_\beta i_\alpha^*\right] \tag{35}$$

The required active (P_{ref}) and reactive (Q_{ref}) powers are used to determine the i_α^* and i_β^* reference currents, then the reference signal generator sends i_α^* and i_β^* as shown in Fig. 6. The reference commands i_α^* and i_β^* are determined using (36):

$$\begin{bmatrix} i_\alpha^* \\ i_\beta^* \end{bmatrix} = \frac{2}{3\left(v_\alpha^2 + v_\beta^2\right)} \begin{bmatrix} v_\alpha & v_\beta \\ v_\beta & -v_\alpha \end{bmatrix} \begin{bmatrix} P_{ref} \\ Q_{ref} \end{bmatrix}. \tag{36}$$

where v_α and v_β are grid voltage in the $\alpha\beta$ reference frame.

V. GSC DC LINK AND CURRENT CONTROL

The dynamics of the three-phase voltage source converter (VSC) connected to the grid through an L filter is expressed via a block diagram in Fig. 8, where C(s) is the controller, G(s) is the PWM dynamic of the VSC, $G_p(s)$ is the VSC plant with the L filter [15].

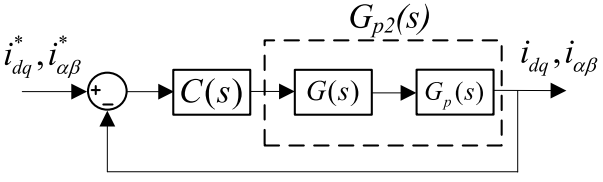

FIGURE 8. Current-controlled VSC control block diagram.

The transfer function $G_p(s)$ is given by (37):

$$G_p(s) = 1/(Ls + R) \tag{37}$$

where: L is the VSC filter; R is filter resistance, Gp2(s) is G(s) and Gp(s) in cascade.

The dynamics of the current of the VSC have no dependency on the frame adopted, but on the parameters of the inductive filter used for coupling the converter and the electric grid according to (37).

Aiming to consider the dynamics of the VSC PWM, which represents a time delay G(s) (equation (38)), the GSC and RSC controllers design were based on the frequency response method [16]:

$$G(s) = (1 - sT)/(1 + sT) \tag{38}$$

where T is the inertia of the PWM converter.

A. CONTROLLERS DESIGN – STRATEGY 1

In strategy 1, PI controllers are adopted. The transfer function for the $C(s)$ controller is given by (39):

$$C(s) = k_p\ (1 + \ 1/T_i/s) \tag{39}$$

The $C(s)$ controller design is determined by open-loop frequency response control of i_d and i_q of GSC in Fig. 8, based on (40) and (41) the parameters T_i and k_p are obtained [17].

$$T_i = 1/\left(\omega_c \tan\left(\pi + G_{p2}(j\omega_c) - PM_d\right)\right) \tag{40}$$

$$k_p = 1/\left(\left|G_{p2}(j\omega_c)\right| |1 - j\omega_c T_i|\right) \tag{41}$$

where ω_c is the gain crossover frequency and PM_d is the phase margin desired.

The literature consider that a well-designed control system has a gain margin (GM) bigger than 6 dB and a phase margin (PM) midway 30° and 60° [18], [19]. Thus, considering a $\omega_c = 16,000$ rad/s and PM_d of 60° the values of $k_p = 120$ and $T_i = 0.0126$ were calculated for the GSC current controllers, as in Fig. 10 (a).

The VSC DC link voltage control diagram is presented in Fig. 9, and enclose PI(s), G_i(s) and G_v(s) which are the controller, the closed-loop of the GSC current and the DC link voltage dynamic respectively, G_{v2}(s) is Gi(s) and G_v(s) cascaded.

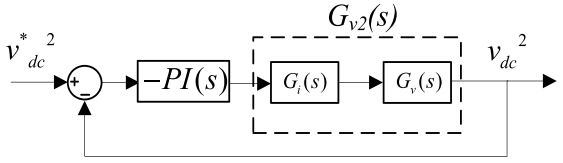

FIGURE 9. Block diagram for the DC-link voltage control loop.

Normally, the interface reactors instantaneous power is neglected in the literature [20]–[22], therefore the simplified model transfer function $G_v(s)$ can be written as [23]:

$$G_v(s) = -(2/C_e)(1/s), \tag{42}$$

where Ce is an equivalent capacitance of the VSC.

From (42), one can observe that the operating point does not affect this model. On the other hand, to derive the precise model, the instantaneous powers of the reactors are considered and the transfer function Gv(s) becomes [15]:

$$G_v(s) = -(2/C_e)(\tau s + 1/s), \tag{43}$$

$$\tau = 2LP_{exto}/3V_s^2 \tag{44}$$

where P_{exto} is active power.

Equation (43) implies the proportionality between τ and the active power flow from the source to the converter. There are 2 operating modes, when $P_{exto} > 0$ and $\tau > 0$ occurs the converter operating mode, if $P_{exto} < 0$ and $\tau < 0$ occurs the rectifier operating mode. If $\tau = 0$, equation (42) becomes a particular case of equation (43).

From the developed technique for the GSC current controllers design and considering open loop in Fig. 9, the parameters T_i and k_p of the DC bus voltage controller are calculated by:

$$T_i = 1/(\omega_c \tan(\pi + G_{v2}(j\omega_c) - PM_d)) \tag{45}$$

$$k_p = 1/(|G_{v2}(j\omega_c)| |1 - j\omega_c T_i|) \tag{46}$$

Considering the VSC DC link voltage controller precise model in (43) the values of $k_p = 0.1401$ and $T_i = 0.0101$ were obtained for the DC link voltage controller through equations (45) and (46) in respect to a PM_d of 60° and $\omega_c = 150$ rad/s as shown in Fig. 10 (b).

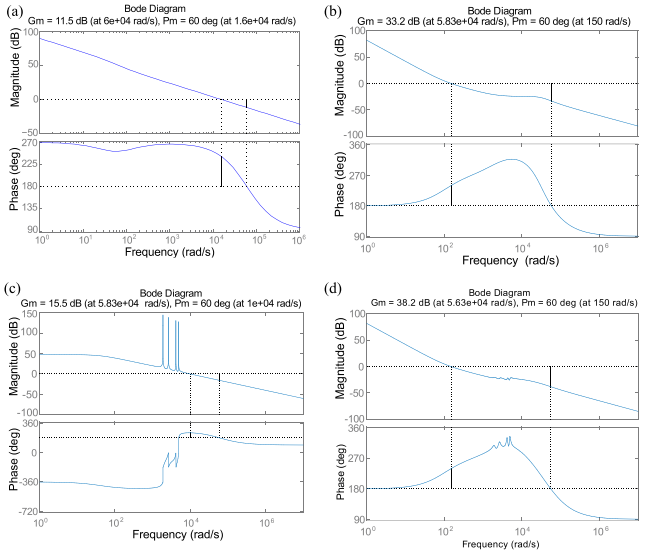

FIGURE 10. Open-loop frequency response control of: i_d and i_q of GSC – strategy 1 (a), DC link voltage control of GSC - strategy 1 (b), i_α and i_β of GSC - strategy 2 (c), DC link voltage control of GSC - strategy 2 (d).

B. CONTROLLERS DESIGN - STRATEGY 2

In this strategy, it was adopted the proportional-multiresonant controller in the $\alpha\beta$ reference frame to compensate four specific harmonic components. A significant feature is that the resonant controller is capable of sufficiently tracking the AC reference current and therefore, can eliminate steady-state

control errors at the selected frequencies. The selected frequencies are at the 5th., 7th., 11th. and 13th. harmonic orders. The transfer function of the $C(s)$ controller is given by (47) [17]:

$$C(s) = k_p + (k_p/T_r) \sum_{h=5,7,11,13} s/(s^2 + (h\omega)^2) \quad (47)$$

for $s = j\omega$, it results:

$$\sum_{h=5,7,11,13} s/(s^2 + (h\omega)^2) = N(s)/D(s) \quad (48)$$

$$C(s) = k_p \left[1 + T_r^{-1} N(s)/D(s)\right] \quad (49)$$

As $D(s)$ is a polynomial of even powers, $Im[D(s)] = 0$. As $N(s)$ is a polynomial of odd powers, thus $Re[N(j\omega)] = 0$. For $s = j\omega$, $D(s)$ and $N(s)$ are written as (50) and (51) respectively.

$$D(j\omega) = \mathrm{Re}\left[D\left(j\omega\right)\right] \quad (50)$$

$$N(j\omega) = j\mathrm{Im}\left[N\left(j\omega\right)\right] \quad (51)$$

$$C(j\omega) = k_p \left\{1 + T_r^{-1} \mathrm{Im}\left[N\left(j\omega\right)\right] / \mathrm{Re}\left[D\left(j\omega\right)\right]\right\} \quad (52)$$

The $C(s)$ controller design is defined as follows in [13], where the parameters T_r and k_r are determined by:

$$T_r = Im\left[N(j\omega_c\right] / (Re\left[D(j\omega_c\right] \tan(PM_d - \angle G_p(j\omega_c) - \pi)) \quad (53)$$

$$k_p = |Re\left[D(j\omega_c)\right]| \left|G_p(j\omega_c)\right|^{-1} / \sqrt{\{Re\left[D(j\omega_c)\right]\}^2 + \left\{T_r^{-1} Im\left[N(j\omega_c)\right]\right\}^2} \quad (54)$$

The values of $k_p = 73.5436$ and $T_r = 0.1187$ of GSC current controllers were calculated for $\omega_c = 10,000$ rad/s and PM_d of 60°, in Fig. 10 (c).

The parameters of the DC link voltage controller are determined by equations (45) and (46), considering open loop in Fig. 9, and the $C(s)$ current controllers design in the strategy 2. The values of $k_p = 0.1417$ and $T_i = 0.0102$ for the DC link voltage controller were obtained for $\omega_c = 150$ rad/s and PM_d of 60° as in Fig. 10(d).

VI. RSC CURRENT CONTROL

The block diagram for the control system of the DFIG rotor currents that pass through the VSC is presented in Fig. 11. The simplified block diagram is composed by a PI(s) controller, the VSC PWM dynamic G(s) and the DFIG plant $G_m(s)$. $G_{m2}(s)$ represents G(s) cascaded with $G_m(s)$. The transfer function $G_m(s)$ is given by (55) [13].

$$G_m\left(s\right) = 1/(\sigma L_r s + R_r), \quad (55)$$

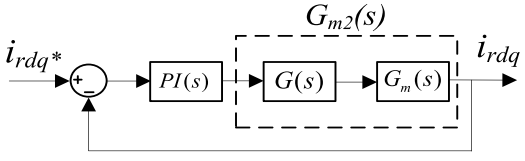

FIGURE 11. Current-controlled VSC control block diagram.

The current controller design of RSC is the identical in both strategies according to the dynamics of the current presented in (55) because the generator parameters are not modified.

From the developed technique for the current controllers design in section 5.1 and considering open loop in Fig. 11, the parameters of the rotor current controllers are given by (56) and (57).

$$T_i = 1/\left(\omega_c \tan\left(\pi + G_{m2}\left(j\omega_c\right) - PM_d\right)\right) \quad (56)$$

$$k_p = 1/\left(\left|G_{m2}\left(j\omega_c\right)\right| \left|1 - j\omega_c T_i\right|\right) \quad (57)$$

Considering a PM_d of 60° and $\omega_c = 500$ rad/s, $k_p = 6.9$ and $T_i = 0.0028$ were calculated for the RSC current controller.

VII. SIMULATION RESULTS

The dynamics of the three-phase voltage source converter (VSC) connected to the The software Matlab/Simulink®with the SimPowerSystem toolbox was used to simulate the system shown in Fig. 1 and to evaluate the proposed control strategies. The system is composed by converters, a DFIG, a balanced three-phase source and a three-phase full bridge rectifier with L_{iL} feeding a resistive load R. The simulation parameters are displayed in the APPENDIX.

The rotor terminals are connected to the electric grid through the back-to-back converter while the stator terminals are directly connected to the electric grid. The control is such that the active and reactive power flow are controlled by the RSC controller and the DC link voltage is regulated by the GSC controller. The GSC controller is also capable of active filtering.

The GSC and RSC reference currents were implemented using PWM on both converters. The software Simulink was used to model the control algorithms for the RSC control (Fig. 3) and the GSC control (Fig. 2, 4 and 6). The current in rotating frame is transformed to an *abc*frame through the *dq-abc* transformation in order to generate the reference currents for the algorithms (Fig. 2 and 4). Also, an $\alpha\beta$-*abc* transformation is employed to produce current reference for the APF (Fig. 6).

The models and controllers used in the simulation were discretized using the Tustin method. The sampling frequency and switching frequencies of the converters used were 30 kHz and 15 kHz respectively. Three different system operation conditions were analyzed. In the first case (case 1), active power is provided by the generator to the grid connected nonlinear load. In cases 2 and 3, the generator provides active power to the same load and simultaneously realizes grid current harmonic filtering, with strategy 1 for case 2 and strategy 2 for case 3.

Case 1: For this case, the DFIG provides electric power and the i_{dr} and i_{qr} current components follow the references i_{drref} and i_{qrref}, as presented in Fig. 12(a), therefore controlling the P_s and Q_s powers (Fig. 12(b)). In this case, there is no power overshoot and the generated power continues stable.

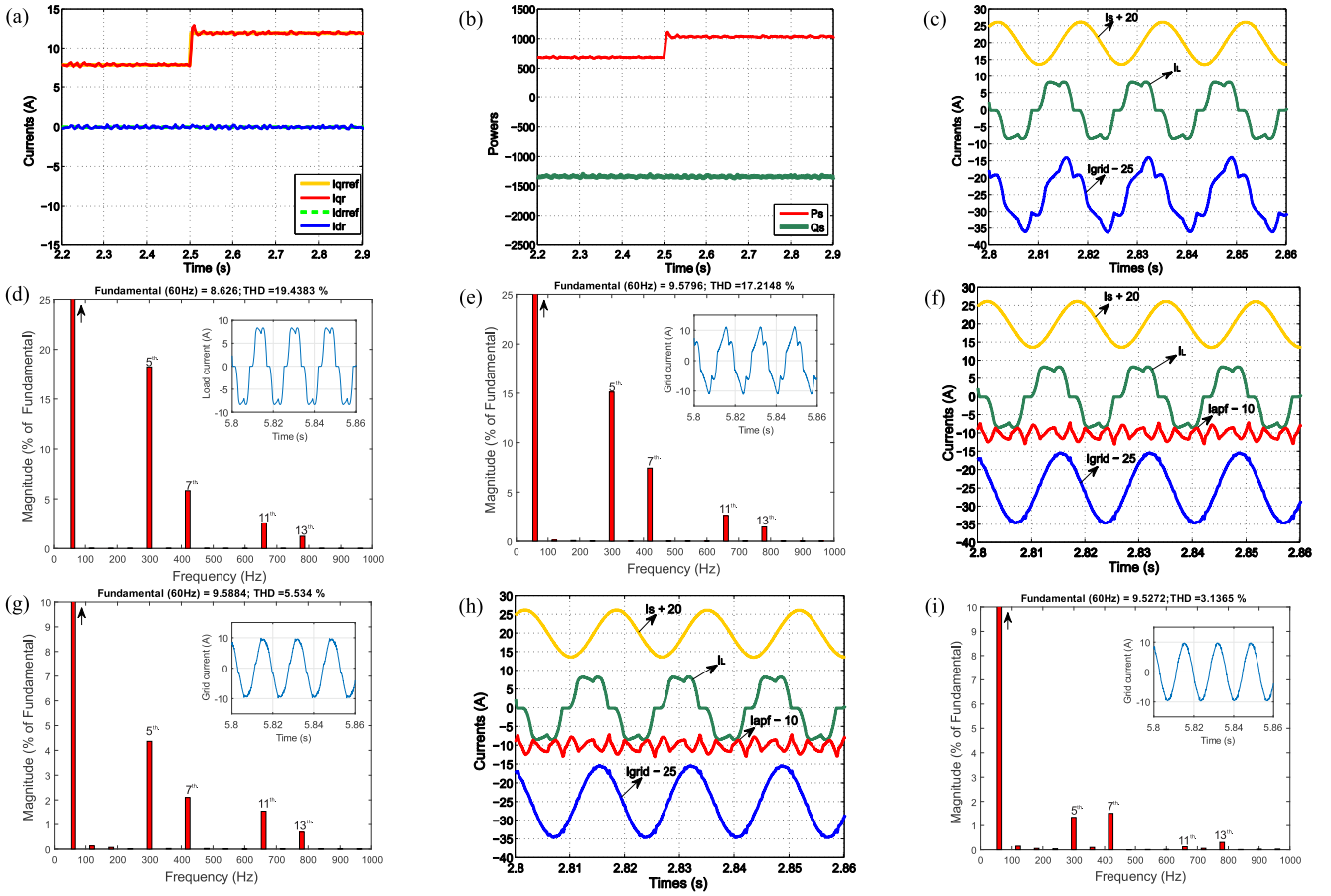

FIGURE 12. Response of control loop of the rotor current controllers i_{rd} and i_{rq} (a), Response of active (P_s) and reactive (Q_s) powers injected in the electric grid (b), Waveforms of grid voltage, DFIG (I_s), load (I_L), electric grid (I_{grid}) currents for the system running in generator mode (c). Load current harmonic spectrum (d), No filtering grid current harmonic spectrum at speed of 178 rad/s (e), Waveforms of DFIG (I_s), load (I_L), active filter (I_{apf}), electric grid currents (I_{grid}) for system running in APF mode – Strategy 1 (f), Active filtering grid current harmonic spectrum with Strategy 1 (g); Waveforms of DFIG (I_s), load (I_L), active filter (I_{apf}), electric grid currents (I_{grid}) for system running in APF mode – Strategy 2 (h), Harmonic spectrum of the grid current with filtering – Strategy 2 (i).

The total harmonic distortion (THD) is calculated through equation (58) aiming to assess the harmonic content [24]:

$$THD\,(\%) = 100.\left(\sqrt{\sum_{h=2}^{50} I_h^2}\right)/I_1 \tag{58}$$

where I_1 is fundamental and I_h are others harmonics components of grid current. Note that the *THD* calculation does not include the inter-harmonics of the electric current.

The current in the nonlinear load is presented in Fig. 12(c). The harmonic spectrum for this current is shown in Fig. 12(d). The THD for this current is 19.43% (Fig. 12(d)). The THD of the PCC current waveform is 17.21% at 178 rad/s (Fig. 12(e)). This value is higher than the accepted value according to the main standards governing the connection of generators to the low voltage electric grid [24]. This grid current THD level can cause voltage distortion to other consumers connected to the PCC. The 5th and 7th odd-order harmonics are the main responsible for the distortion as presented in Fig. 12(e).

Case 2: In case 2, harmonic filtering function is achieved while the generator provides power. The power control behaves similarly to case 1 because in both cases the same RSC control algorithm is used. The generator, load, APF and electric grid currents waveforms are presented in Fig. 12(f). The waveforms are measured while the system operates in harmonic filtering function, feeding a nonlinear load and running at a speed of 178 rad/s.

Differently from the grid current in case 1 (Fig. 12(c)), the grid current in case 2 has sinusoidal behavior (Fig. 12(f)) due to APF harmonic current mitigation. The grid current spectrum without (case 1) and with the active filtering (case 2) show that For this case, the DFIG provides electric power and the i_{dr} and i_{qr} current components follow the references the grid current THD decreases from 17.21% to 5.53% at 178 rad/s (Fig. 12(e) and Fig. 12(g)).

Case 3: Case 3 consists of the generator providing powers and operating in the APF mode using strategy 2. Again, the RSC control algorithm used is the same, thus, the power control behaves similarly to case 1 as shown in Fig. 12(a) and

Fig. 12(b). On the other hand, the grid current (Fig. 12(h)) presents sinusoidal behavior differently from the grid current in case 1 (Fig. 12(c)) due to harmonic current mitigation produced by the control system using strategy 2. The implementation of the harmonic filtering (case 3) decreases the THD from 17,21% to 3,13% at the speed of 178 rad/s compared to case 1 (Fig. 12(e) and 12(i)).

VIII. EXPERIMENTAL RESULTS

An experimental bench was assembled to implement the DFIG system and verify the proposed control schemes. The complete system is composed by a DFIG coupled to a squirrel cage induction motor, power converters, sensors and a control system. The squirrel cage induction machine is controlled by a converter and works as the wind turbine. The reference rotor speed was set to 1700 rpm in the RSC control. A DSP TMS320F28335 was used to implement both the RSC and the GSC control algorithms. The power switches (IGBTs) drivers used were the SEMIKRON SKHI PC22AS. The converters operate at a 15 kHz switching frequency and a 30 kHz sampling frequency.

Case 1: For case 1 the system operates in generating mode. In this case, the system runs at generator mode. The voltage in the DC-link is maintained at 400 V. The rotor currents track the reference currents and the powers are controlled (Fig. 13(a) and 13(b)). The reference current i_{rq} changes from 8A to 12A, while i_{rd} is kept zero, thus the reactive power is delivered by the electric grid. While maintaining the reactive power at the value of −1,300 VAr, the active power was varied from 700W up to 1050W.

The THD of the grid and load currents are 17.34% (Fig. 13(d)) and 20.98% (Fig. 13(c)) respectively. The THD of the electric grid current obtained by simulation and experimental result present small deviation (error = 0.75%), as one can note comparing Fig. 12(e) and Fig. 13(d).

Case 2: For this case, the electric generator provides electric power and the GSC simultaneously performs the APF function. Note that in case 2 there is a three-phase nonlinear load at the PCC. Again, the reference current i_{rd} remains at zero while i_{rq} changes from 8A up to 12A. Thus, the active and reactive powers present similar behavior as in case 1. The generator, electric grid, APF and load currents waveforms are obtained when the system is running in APF mode with strategy 1 as presented in Fig. 13(e). The experimental results are similar to the ones obtained with numerical simulation (section VII.2). The grid current THD is 5.68% (Fig. 13(f)). The electric grid current THD obtained by simulation in Fig. 12(g), section VII.2, is well representative with an error of 2.64% in relation to experimental result, in Fig. 13(f).

Case 3: For case 3, the machine operates as generator and supply electric power while the GSC works as APF. A three-phase nonlinear load is present in the PCC. The same scenario is imposed, the current ird remains null while irq goes from 8A to 12A. Thus, both active and reactive powers exhibit similar behavior to the section VII. The generator, electric grid, APF and load currents waveforms are obtained when the system running in APF mode with strategy 2 and presented in Fig. 13(f). The experimental results are similar to the ones obtained with numerical simulation (section VII). The grid current has for specific frequencies and also eliminates harmonics currents in systems that employ power electronic converters [25]–[27]. The grid current TDH is higher than 5% when the DFIG system works without harmonic current filtering (table 1), it is not according to the IEEE standard in [24]. When strategy 2 is current THD obtained by simulation in section VII.3 is analogous to experimental result with an error of 1.88%.

TABLE 1. THD of grid current when DFIG provides power to the electric grid without or with harmonic filtering (experimental results).

Power (W)	*THD* (%) - *without filtering*	*THD* (%) - strategy 1	*THD* (%) - strategy 2
0	15.66	4.67	2.78
350	16.32	5.05	2.98
750	17.00	5.32	3.09
1050	17.34	5.68	3.18

IX. SUMMARIZING THE COMPARISON BETWEEN THE STRATEGIES

Two wind power system control strategies realize power generation and the grid current harmonic components mitigation.

In strategy 1, the GSC current control uses proportional integral (PI) controllers to model in *dq* frame reference, while in strategy 2, the GSC current control employs proportional multi-resonant controllers to model in $\alpha\beta$ frame reference.

The strategy 1 needs a PLL for synchronize the converter to the power grid, while in strategy 2 the PLL is not necessary. Though, in both strategies the harmonic identification uses the *dq* frame reference. In the two strategies the RSC current control use PI controllers by the rotor current in the *dq* reference frame. Note that the harmonic filtering function and the power control happen simultaneously.

Table 1 presents the grid current THD from experimental tests according to filtering function and power level delivered from the generator to the grid.

The THD of grid current has smaller values when system works with or without harmonic filtering for lower active powers injected to the power grid, in table 1.

At first, all the current required by the load is supplied by the electric grid. When the generator starts injecting active power and harmonic filtering, the load current begins to be supplied by the DFIG. Since the generator is now producing active power, the nonlinear load becomes less dependent on the grid for the required fundamental current.

The GSC supplies only the harmonic components while the fundamental component is provided by both the electric grid and the generator. When the generator increases the active power production, the fundamental current required from the electric grid decreases but the harmonic grid currents are the same, implying in THD increase in the grid current, thus the APF is required. The usage of P-resonant controllers

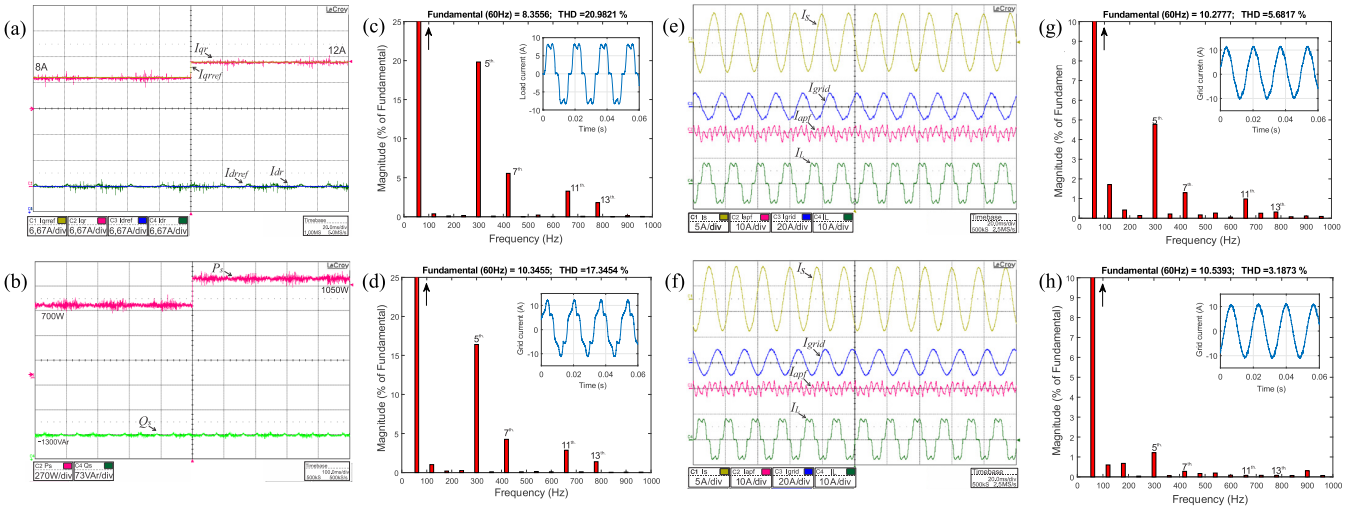

FIGURE 13. **Experimental results: The response of control loop of the rotor currents controllers i_{rd} and irq (a), the response of active (P_s) and reactive (Q_s) powers delivered to the electric grid (b), Harmonic spectrum of load current (c), Harmonic spectrum of the electric grid current without filtering at speed of 178 rad/s (d), The waveforms of DFIG (I_s), electric grid (Igrid), active power filter (Iapf) and load (IL) currents, operating in APF mode - Strategy 1 (e), The harmonic spectrum of the grid current with filtering at speed of 178 rad/s - Strategy 1 (f), The waveforms of DFIG ($I = s$), electric grid (I_{grid}), active power filter (I_{apf}) and load ($I = L$) currents, operating in APF mode - Strategy 2 (g), Harmonic spectrum of the grid current with filtering at speed of 178 rad/s - Strategy 2 (h).**

increase the system bandwidth for specific frequencies and also eliminates harmonics currents in systems that employ power electronic converters [25]–[27].

The grid current TDH is higher than 5% when the DFIG system works without harmonic current filtering (table 1), it is not according to the IEEE standard in [24]. When strategy 2 is used, all operating points of the DFIG/APF system return current THD lower than 5%, complying with the IEEE standard, while strategy 1 attend the standards only when the $P_s = 0$W.

The electric current THD behavior without filtering (case 1) and with active filtering (cases 2 and 3) demonstrate the reduction of electric grid current THD, when the system realizes the harmonic filtering. Odd harmonic components are also reduced in (Fig. 12 (f)) and case 3 (Fig. 12 (h)), thus the components of $5^{th.}$, $7^{th.}$, $11^{th.}$ and $13^{th.}$ orders present smaller magnitude than same components in case 1 (Fig. 12-d).

From results of the THD obtained in the strategies, one can observe that the strategy 2, which uses the P-multiresonant controller, has better effectiveness. This controller responds better to alternate references than the PI controller used in strategy 1, which has insufficient control bandwidth. In the bode diagram shown in Fig. 14, the open loop frequency response of the GSC current controllers for strategies 1(PI(s)) and 2 (C(s)) are observed. In strategy 2, the harmonics components present small magnitude, because these harmonics are compensated with gains higher than in strategy 1. In contrast, the control bandwidth of the PI controller is not sufficient to regulate at the same harmonics components of $5^{th.}$, $7^{th.}$, $11^{th.}$ and $13^{th.}$ orders shown in Fig. 14.

The controller PI used in strategy 1 presents easy design, but its bandwidth is not sufficient for compensating all harmonics components [15]. The P-multiresonant controller (C(s)) designed in strategy 2 is more complex than

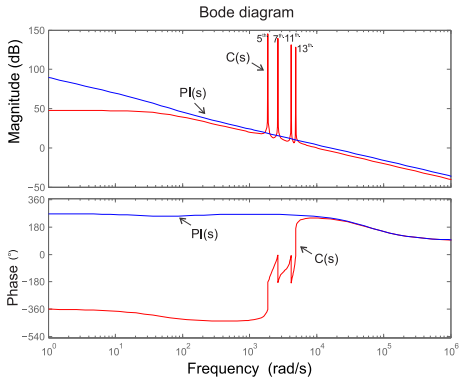

FIGURE 14. **Open loop frequency response of the GSC current control for PI(s) and C(s) controllers.**

PI controller (in strategy 1), however this controller is capable of compensating the selected harmonics components with more efficacy. As a result of strategy 2, the electric grid current presents smaller harmonic content than in the strategy that uses the PI controller.

Thus, the DFIG/APF system with strategy 2 presents better efficacy than strategy 1, considering the same delivered power and the nonlinear load connected to the PCC.

X. CONCLUSION

This paper presented a DFIG driven wind-power system in three operating modes: active power generation mode (case 1) and power control and grid current harmonic filtering mode with two different strategies (cases 2 and 3).

The power generation through DFIG remains equal in all cases. Thus, the stator flux oriented control is employed for power control.

We verified the grid current harmonic spectrum without harmonic filtering function (case 1) and with the harmonic filtering function for the electric grid current (cases 2 and 3)

from both simulation and experimental tests. The numerical simulation results have small deviation from the experimental results, with maximum error of 2.64% in case 2. The experimental results reveal that the grid current THD was reduced from 17.34% (case 1) to 5.68% (case 2) and to 3.18% (case 3). The harmonic filtering strategy integrated into a wind generator with DFIG enhances the power quality in the PCC. The design and implementation methodology of the wind power generation controllers were presented.

Simulation and experimental results using the novel control strategy (strategy 2) proposed confirm the effectiveness of the technique. Strategy 2 presents better effectiveness than strategy 1, being able to reduce the electric current THD for all DFIG/APF system operating points to THD levels that meet the IEEE standard for harmonic control in electrical power systems.

Considering that there is a nonlinear load in the PCC, the grid current THD rises according to the generated power delivered to the grid disregarding the adopted control strategy. The electric grid current THD rise occurs because of the decrease in the electric grid current fundamental component when the generator supplies higher levels of active power. Note that, as expected, even after the harmonic components compensation, the harmonic residues remain in the electric grid.

APPENDIX

DFIG: 2.25 kW, 1750 rpm, 60Hz, 220 V, $L_m = 144.14$mH, $L_{lr} = 11.53$mH, $L_{ls} = 11.53$mH, $R_s = 0.47\ \Omega$, $R_r = 1.31\Omega$; $I_{rotor} = 20.2$ A; $I_{stator} = 8.8$ A.

Nonlinear Load: $R_L = 34\ \Omega$, $L_{iL} = 10$mH.

Converter and Inductive Filter: $C_e = 2250\ \mu$F, $L = 7.5$mH, $R = 0.31\ \Omega$.

Electric Grid: 220V, 60Hz, $L_g = 2.85\mu$H.

REFERENCES

[1] M. Boutoubat, L. Mokrani, M. Machmoum, and F. Auger, "Selective harmonics compensation using a WECS equipped by a DFIG," in *Proc. 38th Annu. Conf. IEEE Ind. Electron. Soc. (IECON)*, Oct. 2012, pp. 745–750.
[2] B. Belmadani, R. Wamkeue, D. Kairus, and M. Benghanem, "Variable structure control of DFIG for wind power generation and harmonic current mitigation," *Adv. Elect. Comput. Eng.*, vol. 10, no. 4, pp. 167–174, 2010.
[3] M. Boutoubat, L. Mokrani, and M. Machmoum, "Control of a wind energy conversion system equipped by a DFIG for active power generation and power quality improvement," *Renew. Energy*, vol. 50, pp. 378–386, Feb. 2013.
[4] M. Kesraoui, A. Chaib, A. Meziane, and A. Boulezaz, "Using a DFIG based wind turbine for grid current harmonics filtering," *Energy Convers. Manage.*, vol. 78, pp. 968–975, Feb. 2013.
[5] A. Gaillard, P. Poure, and M. Machmoum, "Variable speed DFIG wind energy system for power generation and harmonic current mitigation," *Renew. Energy*, vol. 34, no. 6, pp. 1545–1553, Jun. 2009.
[6] D. Kairous, R. Wamkeue, and M. Belmadani, "Towards DFIG control for wind power generation and harmonic current mitigation," in *Proc. CCECE*, May 2010, pp. 1–6.
[7] M. T. Abolhassani, P. Enjeti, and H. A. Toliyat, "Integrated doubly fed electric alternator/active filter (IDEA), a viable power quality solution, for wind energy conversion systems," *IEEE Trans. Energy Convers.*, vol. 23, no. 2, pp. 642–650, Jun. 2008.
[8] H. Akagi, E. H. Watanabe, and M. Aredes, *Instantaneous Power Theory and Applications to Power Conditioning*, 1st ed. Hoboken, NJ, USA: Wiley, 2007.
[9] G. F. Gontijo, C. M. Freitas, R. C. R. da Silva, W. I. Suemitsu, E. H. Watanabe, and M. Aredes, "Control of a DFIG in a wind power system connected to a four-wire grid with power conditioning functionalities," in *Proc. 42nd Annu. Conf. IEEE Ind. Electron. Soc. (IECON)*, Oct. 2016, pp. 2241–2246.
[10] A. B. Moreira, T. A. S. Barros, V. S. C. Teixeira, and E. Ruppert, "Harmonic current compensation and control for wind power generation with doubly fed induction generator," in *Proc. IEEE/IAS Int. Conf. Ind. Appl. (INDUSCON)*, Juiz de Fora, Brazil, 2014, pp. 1–8.
[11] N. K. S. Naidu and B. Singh, "Doubly fed induction generator for wind energy conversion systems with integrated active filter capabilities," *IEEE Trans. Ind. Informat.*, vol. 11, no. 4, pp. 923–933, Aug. 2015.
[12] A. B. Moreira, T. A. S. Barros, Vanessa S. C. Teixeira, and E. Ruppert, "Power control for wind power generation and current harmonic filtering with doubly fed induction generator," *Renew. Energy*, vol. 107, pp. 181–193, Jul. 2017.
[13] B. Singh and J. Solanki, "A comparison of control algorithms for DSTATCOM," *IEEE Trans. Ind. Electron.*, vol. 56, no. 7, pp. 2738–2745, Jul. 2009.
[14] G. Todeschini and A. E. Emanuel, "Wind energy conversion systems as active filters: Design and comparison of three control methods," *IET Renew. Power Gener.*, vol. 4, no. 4, pp. 341–353, Jul. 2010.
[15] A. Yazdani and R. Iravani, *Voltage-Sourced Converters in Power Systems: Modeling, Control, and Applications*. Hoboken, NJ, USA: Wiley, 2012.
[16] S. Buso and P. Mattavelli, *Digital Control in Power Electronics*, 2nd ed. Lincoln, NE, USA: Morgan & Claypool, 2015.
[17] P. S. N. Filho, T. A. dos Santos Barros, M. V. G. Reis, M. G. Villalva, and E. R. Filho, Strategy for modeling a 3-phase grid-tie VSC with LCL filter and controlling the DC-link voltage and output current considering the filter dynamics, in *Proc. IEEE 16th Workshop Control Modeling Power Electron. (COMPEL)*, Jul. 2015, pp. 1–8.
[18] K. Ogata, *Modern Control Engineering*. London, U.K.: Pearson, 2003.
[19] I. D. Landau and G. Zito, *Digital Control Systems: Design, Identification and Implementation*. London, U.K.: Springer, 2006.
[20] R. Pena, R. Cardenas, R. Blasco, G. Asher, and J. Clare, "A cage induction generator using back to back PWM converters for variable speed grid connected wind energy system," in *Proc. 27th Annu. Conf. IEEE Ind. Electron. Soc. (IECON)*, vol. 2, Nov./Dec. 2001, pp. 1376–1381.
[21] C. K. Sao, P. W. Lehn, M. R. Iravani, and J. A. Martinez, "A benchmark system for digital time-domain simulation of a pulse-width-modulated D-STATCOM," *IEEE Trans. Power Del.*, vol. 17, no. 4, pp. 1113–1120, Oct. 2002.
[22] Y. Ye, M. Kazerani, and V. H. Quintana, "Modeling, control and implementation of three-phase PWM converters," *IEEE Trans. Power Electron.*, vol. 18, no. 3, pp. 857–864, May 2003.
[23] A. Yazdani and R. Iravani, "An accurate model for the DC-side voltage control of the neutral point diode clamped converter," *IEEE Trans. Power Del.*, vol. 21, no. 1, pp. 185–193, Jan. 2006.
[24] *IEEE Recommended Practices and Requirements for Harmonic Control in Electrical Power Systems*, IEEE Standard 519-1992, Apr. 1993.
[25] C. Liu, F. Blaabjerg, W. Chen, and D. Xu, "Stator current harmonic control with resonant controller for doubly fed induction generator," *IEEE Trans Power Electron.*, vol. 27, no. 7, pp. 3207–3220, Jul. 2012.
[26] M. Liserre, R. Teodorescu, and F. Blaabjerg, "Multiple harmonics control for three-phase grid converter systems with the use of PI-RES current controller in a rotating frame," *IEEE Trans. Power Electron.*, vol. 21, no. 3, pp. 836–841, May 2006.
[27] V.-T. Phan and H.-H. Lee, "Control strategy for harmonic elimination in stand-alone DFIG applications with nonlinear loads," *IEEE Trans. Power Electron.*, vol. 26, no. 9, pp. 2662–2675, Sep. 2011.

ADSON BEZERRA MOREIRA received the B.Sc. and M.Sc. degrees in electrical engineering from the Federal University of Ceará (UFC), Fortaleza, in 2003 and 2006, respectively, and the Ph.D. degree in electrical engineering from the State University of Campinas, Campinas, Brazil, in 2017. Since 2008, he has been with UFC/Campus Sobral, Sobral, Brazil, where he is currently an Assistant Professor. His research interests include energy efficiency, electric machines, power electronics, electric machine drives, active power filter, and renewable energy (wind generation and solar generation).

TÁRCIO ANDRÉ DOS SANTOS BARROS (S'14–M'17) received the bachelor's degree in electrical engineering from the Federal University of Vale do São Francisco, Petrolina, Brazil, in 2010, and the M.S. and Ph.D. degrees from the University of Campinas, Campinas, Brazil, in 2012 and 2015, respectively, where he was a Researcher under the FAPESP Postdoctoral Program from 2016 to 2017 and he is currently a Professor. He involves in electrical machines, power electronics, and electrical drives. His research interests include machine drives, switched reluctance machines, doubly fed induction generators, and solar energy. He is a member of PELS and the Brazilian Society of Power Electronics.

VANESSA SIQUEIRA DE CASTRO TEIXEIRA was born in Fortaleza/CE, Brazil. She received the B.S. and M.S. degrees in electrical engineering from the Federal University of Ceará, Brazil, in 2004 and 2008, respectively, and the Ph.D. degree from the State University of Campinas, Campinas, Brazil, in 2018, all in electrical engineering. She is currently a Professor of electrical engineering with the Federal University of Ceará, Sobral Campus. Her research interests include energy efficiency, electromagnetic design and modeling of electric machines and innovations in electric machines, and drives systems.

RAMON RODRIGUES DE SOUZA was born in Parintins, Brazil, in 1990. He received the B.S. degree in electrical engineering from Amazonas State University, Manaus, Brazil, in 2012, and the M.Sc. degree in electrical engineering from the University of Campinas, Campinas, Brazil, in 2015, where he is currently pursuing the Ph.D. degree. His research interests include electrical machines, renewable energy, power electronics, active filters, and electric machine drives.

MARCELO VINICIUS DE PAULA (S'17) received the B.S. degree in electrical engineering from the Federal University of Goiás, Goiânia, Brazil, in 2016, and the M.Sc. degree in electrical engineering from University of Campinas, Campinas, Brazil, in 2018, where he is currently pursuing the Ph.D. degree under the CNPq Scholarship Program. He involves in the areas of electric machines and drives, power electronics, and electric vehicles. His research interests include torque ripple minimization, switched reluctance machine drives, electric vehicles, and renewable energy.

ERNESTO RUPPERT FILHO received the B.S. degree in electrical engineering and the M.S. and Ph.D. degrees from the University of Campinas (UNICAMP), Campinas, Brazil, in 1971, 1974, and 1983, respectively, where he was with the Electrical and Computer Engineering School, from 1972 to 1978 as an Assistant Professor of electromechanical energy conversion. From 1979 to 1983, he was with General Electric, Brazil, as an Application Engineer dedicated to large motors, generators, designing large induction, and synchronous motors. From 1983 to 1989, he was with Vigesa Heavy Equipment, Brazil, designing very large hydrogenerators and performing commissioning tests on hydropower plants in Brazil. He is currently a Full Professor with the Electrical and Computer Engineering School, UNICAMP, researching and teaching in electrical machines, power electronics, drives, and electrical power systems.